

Attention Guided Network for Salient Object Detection in Optical Remote Sensing Images^{*}

Yuhan Lin¹, Han Sun¹, Ningzhong Liu¹, Yetong Bian¹, Jun Cen¹, and Huiyu Zhou²

¹ College of Computer Science and Technology, Nanjing University of Aeronautics and Astronautics, Nanjing, China

Email: sunhan@nuaa.edu.cn

² School of Computing and Mathematical Sciences, University of Leicester, Leicester LE1 7RH, UK

Abstract. Due to the extreme complexity of scale and shape as well as the uncertainty of the predicted location, salient object detection in optical remote sensing images (RSI-SOD) is a very difficult task. The existing SOD methods can satisfy the detection performance for natural scene images, but they are not well adapted to RSI-SOD due to the above-mentioned image characteristics in remote sensing images. In this paper, we propose a novel Attention Guided Network (AGNet) for SOD in optical RSIs, including position enhancement stage and detail refinement stage. Specifically, the position enhancement stage consists of a semantic attention module and a contextual attention module to accurately describe the approximate location of salient objects. The detail refinement stage uses the proposed self-refinement module to progressively refine the predicted results under the guidance of attention and reverse attention. In addition, the hybrid loss is applied to supervise the training of the network, which can improve the performance of the model from three perspectives of pixel, region and statistics. Extensive experiments on two popular benchmarks demonstrate that AGNet achieves competitive performance compared to other state-of-the-art methods. The code will be available at <https://github.com/NuaaYH/AGNet>.

Keywords: Salient object detection · Optical remote sensing images · Position enhancement stage · Detail refinement stage.

1 Introduction

Salient object detection (SOD) is used to simulate the human visual attention mechanism, which helps machine automatically search for the most attractive areas or objects in an image.

In the early days, the traditional methods for SOD are based on hand-crafted features. Such methods can meet the performance requirements of SOD tasks in

^{*} This work is supported in part by the Fundamental Research Funds for the Central Universities of China under Grant NZ2019009.

specific scenarios, which also have the advantages of fast speed and convenient deployment. However, when application environment expands to a wide variety of scenarios, traditional methods do not have satisfactory generalization. In 2015, the SOD model was combined with deep learning technique and convolutional neural network (CNN) for the first time, which aroused the interest of researchers in the topic of CNN-based SOD methods.

At the present time, there has been a lot of excellent work on SOD tasks in natural scene images (NSIs) such as GateNet [20], F3Net [14], LDF [15], GCPANet [1]. However, as an emerging topic of saliency detection, the researches on SOD in optical remote sensing images (RSIs) is still relatively rare. Compared with NSIs, remote sensing images bring us more challenges. Specifically, RSIs are usually taken from a high altitude with a bird’s-eye view through equipments such as aerial cameras or satellites, thus the location of salient objects may appear in various places in the frame. Meanwhile, various scales, complex shapes and indistinct boundaries are the unique features of objects in RSIs, which also hinder the accurate prediction of object details. Since the RSI-SOD datasets were constructed and opened, there have been some promising attempts to solve SOD tasks on remote sensing images, e.g, DAFNet [19], EMFINet [22], SARNet [5]. But none of them can solve the above-mentioned problems well, which includes the optimization of object positioning and object details.

As another huge vision task topic, attention mechanism and salient object detection have many similarities. Over the years, the attention mechanism has been widely used in SOD models and proved to be an extremely effective solution. In this paper, we aim at designing an attention guided network for accurate salient object detection in optical RSIs, called AGNet. To obtain accurate location prediction for salient objects, we propose a position enhancement stage including a semantic attention module and a contextual attention module, which provide the network with attention-guiding information from global semantic and local context perspectives, respectively. In order to obtain a more refined and complete saliency map, a self-refinement module is designed to build the detail refinement stage. The self-refinement module employs attention and reverse attention mechanisms to mine object details in high-confidence and low-confidence regions, thereby gradually improving the prediction results. At last, we evaluate the effectiveness of the proposed network.

2 Related Work

2.1 Attention Mechanism for SOD

In recent years, the attention mechanism is utilized to promote the performance of SOD models to a higher level. Zhao et al. [20] proposes a simple gate network to filter the noise in the encoder feature map and consider the difference in contributions from different encoder blocks. Wu et al. [16] designs a holistic attention module to expand the coverage of the initial saliency map, which helps to segment the entire salient object and optimize the boundaries. Yang et al. [18]

designs a branch-wise attention module to adaptively aggregate multi-scale features so that salient objects can be efficiently localized and detected. Tang et al. [10] proposes a novel non-local cross-level attention, which can capture long-range feature dependencies to enhance the discriminative ability of complete salient objects. And Wang et al. [13] presents a pyramid attention structure to enable the network to pay more attention to saliency regions while exploiting multi-scale saliency information.

2.2 Salient Object Detection for RSIs

As we know, the RSI-SOD methods based on deep learning have become the main research idea since 2019. Zhang et al. [19] proposes a dense attention flow network, in which attention information flows from shallow layers to deep layers to guide the generation of high-level feature maps. Cong et al. [2] presents a graph structure-based reasoning module and a parallel multi-scale attention module, which greatly improve the accuracy and completeness of the saliency map. Zhou et al. [22] uses three encoders with different input scales to extract and fuse multi-scale features, and then introduces the guidance of edge information to obtain high-quality saliency maps. Huang et al. [5] integrates multiple high-level features to locate the object position and feed back the high-level features into the stage of shallow feature fusion. And in [11], a joint learning scheme based on bidirectional feature transformation is proposed to simultaneously optimize the boundaries and regions of salient objects.

In general, since the above deep learning-based RSI-SOD methods have made great progress, these solutions still show unsatisfactory performance when dealing with some difficult samples in Fig. 6. In our AGNet, we design an intuitively more natural method according to the image features of RSIs, which is implemented by position enhancement stage and detail refinement stage.

3 Approach

In this section, we will specify the details of the proposed network. The overall framework of AGNet is given in Fig. 1. From the figure, it is clear that the inference process of the proposed network consists of three main parts: feature encoding backbone, position enhancement stage and detail refinement stage. In the following, the above three components will be discussed in turn. Finally, we will also present the design of the used hybrid loss.

3.1 Feature Encoding Backbone

In this paper, we adopt the widely used Res2Net-50 [3] as the feature encoding backbone of AGNet. To reduce the computational complexity and the overall number of parameters in our network, a 1×1 convolutional layer is used to perform channel downscaling on the five convolutional block outputs of Res2Net.

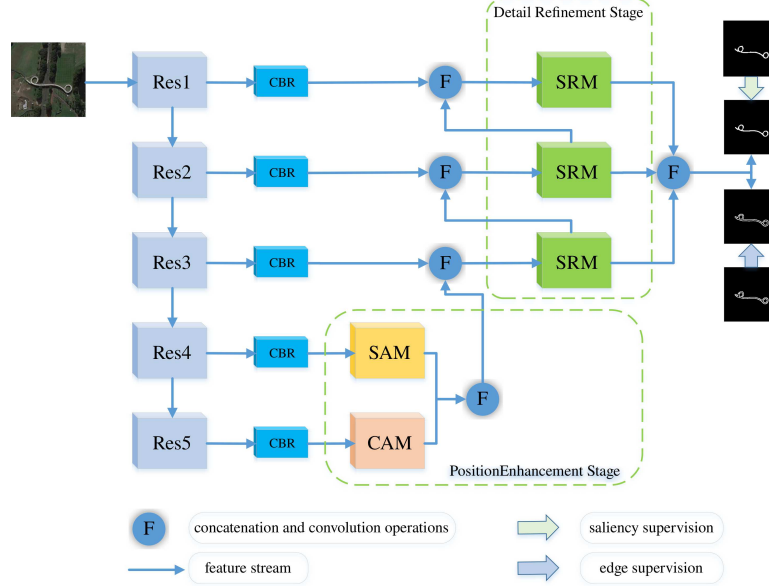


Fig. 1. The architecture of AGNet. CBR refers to the combination of convolutional layer, batch normalization operation, and activation function. SAM means semantic attention module, CAM denotes contextual attention module, and SRM refers to self-refinement module.

At last, all the five groups of feature maps are converted to 128 channels and ready for the next processing step. This process can be formulated as:

$$F_i = \text{relu}(\text{bn}(\text{conv}_{1 \times 1}(f_i))), i = 1 \dots 5 \quad (1)$$

in which $\text{conv}_{1 \times 1}$ denotes the 1×1 convolution operation, bn refers to batch normalization operation, and relu denotes the ReLU activation function. These series of operations will be represented by CBR in this paper.

3.2 Position Enhancement Stage

Inspired by the coarse-to-fine strategy, we propose a position enhancement stage to locate potentially salient object position in the deep feature map. Specifically, the semantic attention module (SAM) is proposed to model semantic relations between different channels on the fourth layer feature map and the contextual attention module (CAM) is designed to estimate the accurate location information of salient objects on the last layer.

Semantic Attention Module. SENet [4] is the most widely used method for calculating channel attention. However, we think that the dimensionality

reduction of channels in SENet will have the side effect of making some semantic information lost. Also, capturing the dependencies between all channels is inefficient and unnecessary [12]. Therefore, a novel semantic attention module without dimensionality reduction is designed in Fig. 2, which can be efficiently implemented via one-dimensional group convolution.

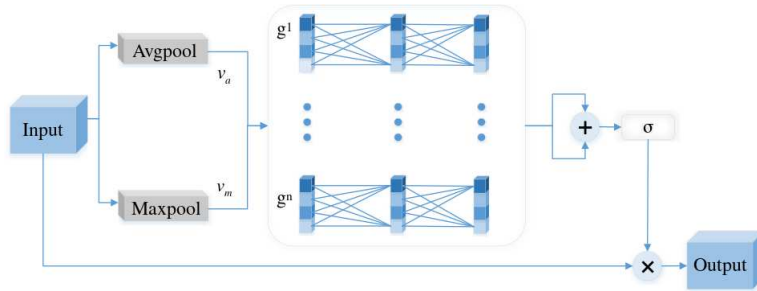


Fig. 2. The architecture of SAM.

Considering that the fourth layer feature map already has a large enough receptive field to describe the semantic information, we use this feature map as input to SAM. First, global average pooling and global maximum pooling are used on the feature map to obtain a global semantic representation of the features, denoted as v_a and v_m . Then, we design a unique method for computing channel attention based on group convolution. Specifically, the above two channel vectors are used to compute local semantic correlations by two one-dimensional group convolutional layers. Each one-dimensional convolution kernel is computed with adjacent channel features, and thus the convolution results can reflect local cross-channel semantic interactions. In this paper, SAM is able to provide the maximum contribution to the network when we set the number of groups to 8. The semantic attention can be formulated as:

$$att = \sigma(gconv_{1 \times 1}(avgpool(f_4)) + gconv_{1 \times 1}(maxpool(f_4))) \quad (2)$$

where σ denotes the sigmoid activation function, $gconv_{1 \times 1}$ denotes the two 1×1 group convolutional layers, $avepool$ and $maxpool$ are the average-pooling and max-pooling in spatial dimension, respectively.

Contextual Attention Module. In RSIs, the location of the salient object is more randomly distributed than in NSIs, such as the center of the view or different corners of the image. Therefore, the contextual attention module is proposed to guide the network to provide the most accurate object position in the deepest layer.

As shown in Fig. 3, unlike previous spatial attention, our CAM calculates the saliency of the location from the channel dimension and the local spatial dimension, respectively. Specifically, one branch performs maximum pooling and

average pooling on the input in the channel dimension, and then cascades the two single-channel feature maps to generate a spatial attention map by convolutional fusion. The other branch computes an attention map directly on the input using 3×3 convolution, which reflects the influence of neighboring pixels on the saliency of a location in the local spatial dimension. The contextual attention can be formulated as:

$$att1 = \sigma(\text{conv}_{3 \times 3}(\text{cat}(\text{max}(f_5), \text{avg}(f_5)))) \quad (3)$$

$$att2 = \sigma(\text{conv}_{3 \times 3}(f_5)) \quad (4)$$

in which *avg* and *max* are the average-pooling and max-pooling in channel dimension, *cat* denotes feature concatenation along channel axis.

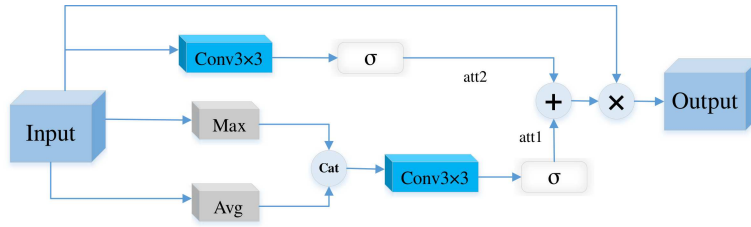


Fig. 3. The architecture of CAM.

3.3 Detail Refinement Stage

As shown in most researches, the shallow features of the network often tend to provide some additional information in terms of local details to the final prediction results. In this section, we will introduce the most critical component of the detail refinement stage, the self-refinement module (SRM), as shown in Fig. 4.

Specifically, the input to each SRM are the fused feature map, which are obtained from the deep feature of the previous layer and shallow feature of the corresponding layer. Subsequently, the convolution operation is used to compute the attention map reflecting the salient regions. At the same time, we invert this attention map to obtain the reverse attention map, which reflects some low-confidence regions ignored by the network. These two attention maps are multiplied with the fused feature map to guide the network to further mine the saliency information from the high-confidence salient regions and the low-confidence background regions. Finally, the two results are summed and fused by the convolutional layer to obtain the output of the SRM. This process can be formulated as:

$$att = \sigma(\text{conv}_{1 \times 1}(f)), att.r = 1 - att \quad (5)$$

$$F = cbr(cbr(att * f) + cbr(att_r * f)) \quad (6)$$

At last, to fully utilize the effect of SRM, the results of the three SRM modules are integrated to obtain the final prediction map of the network by concatenation and convolution operations, as shown in Fig. 1.

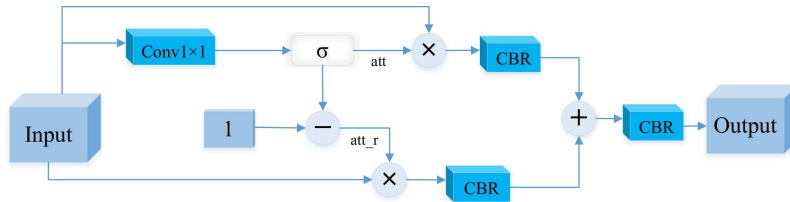


Fig. 4. The architecture of SRM.

3.4 Hybrid Loss of AGNet

In this paper, the widely used cross-entropy loss, IoU loss and recent F-value loss are introduced into hybrid loss to supervise the training of the network from the perspectives of pixels, regions, statistics. Furthermore, edge information is also added to the loss function. In the end, the total loss of the network can be described by the following equation:

$$loss = loss_{bce} + \lambda \cdot loss_{iou} + loss_f \quad (7)$$

$$Loss = loss(P, G_p) + \mu \cdot loss(E, G_e) \quad (8)$$

where λ and μ are hyperparameters that balance the contributions of the three losses and the contributions of the two supervised objects. Empirically, we set $\lambda = 0.6$ and $\mu = 0.5$.

4 Experiment

4.1 Implementation Details

For the EORSSD [19] dataset and ORSSD [6] dataset, we expand their training sets to 11200 and 4800 samples by random flipping and random rotating. We train the proposed AGNet using the adam optimizer with initial learning rate of $1e-4$, weight decay of $5e-4$, and batch size of 8. Cosine annealing decay strategy is adopted to adjust the learning rate and the minimum learning rate is set to $1e-5$. Our network is totally trained for 60 epochs and the input size is 224×224 . For a fair comparison with other methods, four commonly used metrics including the mean absolute error (MAE), mean F-measure (mF), S-measure (Sm) and mean E-measure (mE) are adopted to evaluate the model performance as suggested in [5].

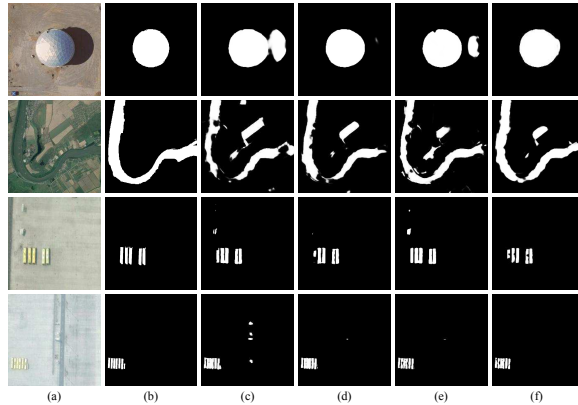


Fig. 5. Comparison of predictions among different networks. (a) Image; (b) Ground truth; (c) Baseline; (d) Baseline+PES; (e) Baseline+DRS; (f) Baseline+PES+DRS.

4.2 Ablation Studies

To demonstrate the effectiveness of the proposed method with convincing data, a series of ablation experiments are presented in this section. The same experimental parameter settings are used throughout the experiment. The qualitative comparison and quantitative comparison are shown in Fig. 5 and Table 1. Specifically, Baseline denotes the U-shaped model with Res2Net-50 as the backbone, PES means the position enhancement stage and DRS refers to the detail refinement stage.

Effectiveness of PES. From Table 1, it can be found that the addition of PES makes the performance of the network have obvious improvements in three main metrics, such as a gain of 0.83% in mF. The effectiveness of PES can be more thoroughly demonstrated in Fig. 5. The fourth column of each row is the saliency map predicted by the model combined with PES on the basis of the baseline. For example, the pictures in the first and second rows in Fig. 5 are representative of challenging scenes in the EORSSD dataset. The salient object in the image of the first row is accompanied by interference information such as shadows, while in the image of the second row, the color and texture features of the river are extremely similar to its surroundings, which can easily guide the network to output wrong results. Thanks to our proposed PES, the model has the ability to remove the background interference and accurately locate the object area, as shown in the third and fourth columns in Fig. 5.

Effectiveness of DRS. To prove the effectiveness of our DRS, we additionally train with a combination of baseline and DRS. The trained model shows the contribution of DRS to the network in Table 1, such as a 0.5% improvement on mF. The third and fourth rows of images in Fig. 5 are used to illustrate the

effectiveness of DRS. As can be seen from the fifth column of Fig. 5, the gaps between closely spaced vehicles are more apparent compared to the baseline, while the shapes of the vehicles are more fully highlighted. This change is because DRS improves the prediction quality of the object details by the network. Our method can refine and supplement the details of salient objects, which is helpful for the application of RSI-SOD in earth observation, object counting, etc.

Table 1. Quantitative evaluation of ablation studies on the EORSSD dataset.

Methods	EORSSD		
	mF \uparrow	mE \uparrow	Sm \uparrow
Baseline	0.8613	0.9554	0.9229
Baseline+PES	0.8696	0.9599	0.9248
Baseline+DRS	0.8663	0.9578	0.9247
Baseline+PES+DRS	0.8736	0.9614	0.9284

4.3 Comparison with State-of-the-arts

To demonstrate the validity of our proposed network, we compare the proposed method against other fourteen current state-of-the-art (SOTA) methods, including eight SOD methods for NSIs (i.e., ITSD [21], LDF [15], MINet [9], GC-PANet [1], GateNet [20], F3Net [14], PA-KRN [17] and SUCA [8]), and six recent SOD methods for optical RSIs (i.e., CorrNet [7], DAFNet [19], EMFINet [22], LVNet [6], MJRBM [11] and SARNet [5]). All NSI-SOD methods are retrained using the original code projects published by their authors. For RSI-SOD methods, we use the saliency maps provided on the corresponding methods on github. Table 2 and Fig. 6 show the comparison of the different methods on the four metrics and visualization results, respectively.

Quantitative comparison. In Table 2, we report the mF, mE, Sm, MAE of our method and fourteen other methods on two RSI-SOD datasets. Compared with other RSI-SOD methods, our method shows impressive performance. Specifically, on the EORSSD dataset, AGNet is much higher than the second-ranked method in mF, mE, e.g., mF: 0.8736 (AGNet) v.s. 0.8690 (CorrNet), and mE: 0.9614 (AGNet) v.s. 0.9512(CorrNet). Meanwhile, on MAE, our method is only slightly weaker than DAFNet by a gap of 0.0009. While on the ORSSD dataset, our method ranks first on mF, mE and MAE. Although our method fails to achieve the best score on both datasets on Sm, our method outperforms by achieving more impressive performance with smaller parameters, e.g., param: 26.60M (AGNet) vs 107.26M (EMFINet). And our AGNet also beats SARNet with the same scale of parameters, the former has about 26M and the latter has 40M. In competition with all NSI-SOD methods, our model and most RSI-SOD methods are a lot ahead of them, which further demonstrates the necessity of specially designing the model for the SOD of optical RSIs.

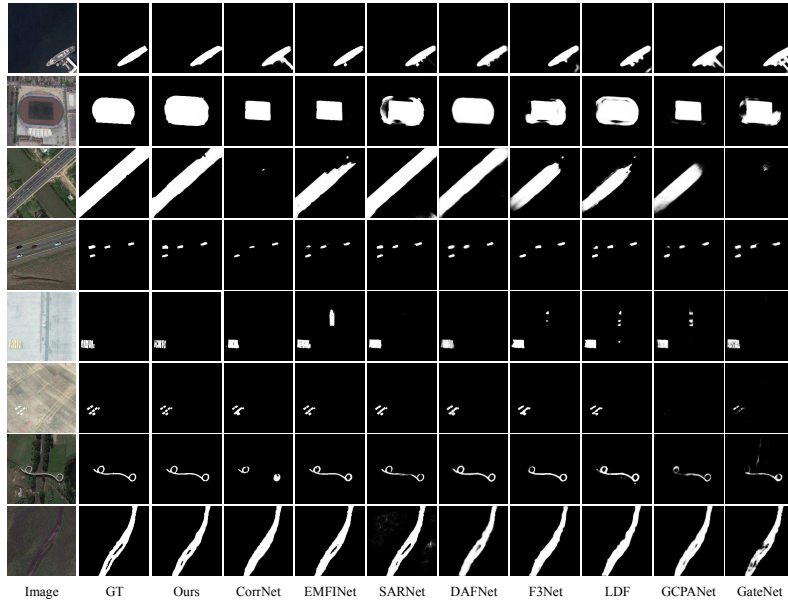


Fig. 6. Visual comparisons of different methods

Table 2. Quantitative evaluation. The best three results are highlighted in red, blue, green.

Methods	type	EORSSD				ORSSD			
		mF \uparrow	MAE \downarrow	Sm \uparrow	mE \uparrow	mF \uparrow	MAE \downarrow	Sm \uparrow	mE \uparrow
ITSD	NSI	0.8313	0.0109	0.9043	0.9265	0.8590	0.0172	0.9056	0.9410
LDF	NSI	0.8317	0.0087	0.9078	0.9464	0.8779	0.0137	0.9143	0.9518
MINet	NSI	0.8233	0.0097	0.9049	0.9190	0.8622	0.0153	0.9040	0.9355
GCPANet	NSI	0.7968	0.0104	0.8855	0.8993	0.8488	0.0177	0.9005	0.9253
GateNet	NSI	0.8314	0.0099	0.9090	0.9238	0.8769	0.0144	0.9192	0.9472
PA-KRN	NSI	0.8434	0.0109	0.9194	0.9416	0.8824	0.0145	0.9243	0.9566
F3Net	NSI	0.8164	0.0088	0.9030	0.9401	0.8677	0.0155	0.9160	0.9538
SUCA	NSI	0.8040	0.0102	0.8971	0.9131	0.8347	0.0150	0.8992	0.9349
CorrNet	RSI	0.8690	0.0087	0.9297	0.9512	0.9077	0.0107	0.9405	0.9687
DAFNet	RSI	0.8135	0.0060	0.9175	0.9295	0.8578	0.0111	0.9186	0.9496
EMFNet	RSI	0.8601	0.0079	0.9307	0.9445	0.9083	0.0104	0.9435	0.9662
LVNet	RSI	0.7488	0.0146	0.8639	0.8729	0.8107	0.0211	0.8807	0.9204
MJRBM	RSI	0.8162	0.0105	0.9068	0.9087	0.8679	0.0151	0.9190	0.9338
SARNet	RSI	0.8625	0.0091	0.9284	0.9482	0.8942	0.0105	0.9361	0.9596
AGNet	RSI	0.8736	0.0069	0.9284	0.9614	0.9109	0.0093	0.9392	0.9707

Qualitative comparison. In Fig. 6, we show the saliency maps for the more difficult test samples. From the visual analysis of the saliency maps in the first to third rows, AGNet outperforms other methods when dealing with multi-scale objects, which is exactly the benefit of a powerful multi-scale feature extractor

and multi-layer feature fusion strategy. The images in the fourth to sixth rows involve multiple small salient objects, which is a challenging problem in the RSI-SOD task. Our method can detect all salient objects and get refined segmentation results. For example, there are seven circular buildings in the image in the sixth row, all of which are clearly marked by our method with the help of PES. But other methods can only detect a part of the buildings, or make objects blend together, such as GateNet and DAFNet. In the last two rows in Fig. 6, we present the performance of all methods when encountering slender or complex-structured objects. For the ring-shaped buildings in the seventh row, our method provides the most complete and clear detection results due to the effect of DRS. For the two lands surrounded by the river in the eighth row, other methods either conflate them with the river or only show a hole in the saliency map, while our method successfully recognizes the two lands as the background, which further confirms the importance of self-refinement for the RSI-SOD task.

5 Conclusion

In this paper, a novel attention-guided network is proposed to solve the RSI-SOD task. To enhance the detection quality of salient object position, a semantic attention module and a contextual attention module are jointly used to guide the network to detect coarse but accurate object locations. In order to make the details of the object more refined and complete, a self-refinement module is designed to refine the feature map from high-confidence and low-confidence regions. Finally, an efficient hybrid loss is employed in the training of the network to boost performance. Experimental results demonstrate the robustness of our method in dealing with multi-scale objects, multiple small objects, and objects with complex structures. In the future, we will try to design a high-precision and lightweight network structure to further promote the application of the RSI-SOD model in real life.

References

1. Chen, Z., Xu, Q., Cong, R., Huang, Q.: Global context-aware progressive aggregation network for salient object detection. In: Proceedings of the AAAI conference on artificial intelligence. vol. 34, pp. 10599–10606 (2020)
2. Cong, R., Zhang, Y., Fang, L., Li, J., Zhang, C., Zhao, Y., Kwong, S.: Rrnet: Relational reasoning network with parallel multi-scale attention for salient object detection in optical remote sensing images. *IEEE Transactions on Geoscience and Remote Sensing* (2021)
3. Gao, S.H., Cheng, M.M., Zhao, K., Zhang, X.Y., Yang, M.H., Torr, P.: Res2net: A new multi-scale backbone architecture. *IEEE transactions on pattern analysis and machine intelligence* **43**(2), 652–662 (2019)
4. Hu, J., Shen, L., Sun, G.: Squeeze-and-excitation networks. In: Proceedings of the IEEE conference on computer vision and pattern recognition. pp. 7132–7141 (2018)
5. Huang, Z., Chen, H., Liu, B., Wang, Z.: Semantic-guided attention refinement network for salient object detection in optical remote sensing images. *Remote Sensing* **13**(11), 2163 (2021)

6. Li, C., Cong, R., Hou, J., Zhang, S., Qian, Y., Kwong, S.: Nested network with two-stream pyramid for salient object detection in optical remote sensing images. *IEEE Transactions on Geoscience and Remote Sensing* **57**(11), 9156–9166 (2019)
7. Li, G., Liu, Z., Bai, Z., Lin, W., Ling, H.: Lightweight salient object detection in optical remote sensing images via feature correlation. *IEEE Transactions on Geoscience and Remote Sensing* (2022)
8. Li, J., Pan, Z., Liu, Q., Wang, Z.: Stacked u-shape network with channel-wise attention for salient object detection. *IEEE Transactions on Multimedia* **23**, 1397–1409 (2020)
9. Pang, Y., Zhao, X., Zhang, L., Lu, H.: Multi-scale interactive network for salient object detection. In: *Proceedings of the IEEE/CVF conference on computer vision and pattern recognition*. pp. 9413–9422 (2020)
10. Tang, L., Li, B.: Class: Cross-level attention and supervision for salient objects detection. In: *Proceedings of the Asian Conference on Computer Vision* (2020)
11. Tu, Z., Wang, C., Li, C., Fan, M., Zhao, H., Luo, B.: Orsi salient object detection via multiscale joint region and boundary model. *IEEE Transactions on Geoscience and Remote Sensing* (2021)
12. Wang, Q., Wu, B., Zhu, P., Li, P., Zuo, W., Hu, Q.: Eca-net: Efficient channel attention for deep convolutional neural networks. In: *2020 IEEE/CVF Conference on Computer Vision and Pattern Recognition (CVPR)*. pp. 11531–11539 (2020)
13. Wang, W., Zhao, S., Shen, J., Hoi, S.C., Borji, A.: Salient object detection with pyramid attention and salient edges. In: *Proceedings of the IEEE/CVF Conference on Computer Vision and Pattern Recognition*. pp. 1448–1457 (2019)
14. Wei, J., Wang, S., Huang, Q.: F³net: fusion, feedback and focus for salient object detection. In: *Proceedings of the AAAI Conference on Artificial Intelligence*. vol. 34, pp. 12321–12328 (2020)
15. Wei, J., Wang, S., Wu, Z., Su, C., Huang, Q., Tian, Q.: Label decoupling framework for salient object detection. In: *Proceedings of the IEEE/CVF conference on computer vision and pattern recognition*. pp. 13025–13034 (2020)
16. Wu, Z., Su, L., Huang, Q.: Cascaded partial decoder for fast and accurate salient object detection. In: *Proceedings of the IEEE/CVF conference on computer vision and pattern recognition*. pp. 3907–3916 (2019)
17. Xu, B., Liang, H., Liang, R., Chen, P.: Locate globally, segment locally: A progressive architecture with knowledge review network for salient object detection. In: *Proceedings of the AAAI Conference On Artificial Intelligence*. pp. 1–9 (2021)
18. Yang, S., Lin, W., Lin, G., Jiang, Q., Liu, Z.: Progressive self-guided loss for salient object detection. *IEEE Transactions on Image Processing* **30**, 8426–8438 (2021)
19. Zhang, Q., Cong, R., Li, C., Cheng, M.M., Fang, Y., Cao, X., Zhao, Y., Kwong, S.: Dense attention fluid network for salient object detection in optical remote sensing images. *IEEE Transactions on Image Processing* **30**, 1305–1317 (2020)
20. Zhao, X., Pang, Y., Zhang, L., Lu, H., Zhang, L.: Suppress and balance: A simple gated network for salient object detection. In: *European conference on computer vision*. pp. 35–51. Springer (2020)
21. Zhou, H., Xie, X., Lai, J.H., Chen, Z., Yang, L.: Interactive two-stream decoder for accurate and fast saliency detection. In: *Proceedings of the IEEE/CVF Conference on Computer Vision and Pattern Recognition*. pp. 9141–9150 (2020)
22. Zhou, X., Shen, K., Liu, Z., Gong, C., Zhang, J., Yan, C.: Edge-aware multiscale feature integration network for salient object detection in optical remote sensing images. *IEEE Transactions on Geoscience and Remote Sensing* (2021)